A reliable and replicable test protocol for the mechanical evaluation of synthetic meshes

journal of the mechanical behavior of biomedical materials 144 (2023) 105987

Contents lists available at ScienceDirect

Journal of the Mechanical Behavior of Biomedical Materials

journal homepage: www.elsevier.com/locate/jmbbm

A reliable and replicable test protocol for the mechanical evaluation of synthetic meshes

Vittoria Civilini [a,b,*], Vincenzo Giacalone [a,b], Alberto L. Audenino [a,b], Mara Terzini [a,b]

[a] Department of Mechanical and Aerospace Engineering, Politecnico di Torino, 10129, Turin, Italy
[b] Polito[BIO]Med Lab, Politecnico di Torino, 10129, Turin, Italy

ARTICLE INFO

Keywords:
Hernia meshes
Urogynecologic devices
Standard test protocol
Mechanical characterization
In vitro test

ABSTRACT

Despite the worldwide spread of surgical meshes in abdominal and inguinal surgery repair, the lack of specific standards for mechanical characterization of synthetic meshes, used in hernia repair and urogynecologic surgery, makes performance comparison between prostheses undoubtedly difficult. This consequently leads to the absence of acknowledged specifications about the mechanical requirements that synthetic meshes should achieve in order to avoid patient discomfort or hernia recurrences.

The aim of this study is to provide a rigorous test protocol for the mechanical comparison between surgical meshes having the same intended use. The test protocol is composed of three quasi-static test methods: (1) ball burst test, (2) uniaxial tensile test, and (3) suture retention test. For each test, post-processing procedures are proposed to compute relevant mechanical parameters from the raw data. Some of the computed parameters, indeed, could be more suitable for comparison with physiological conditions (e.g., membrane strain and anisotropy), while others (e.g., uniaxial tension at rupture and suture retention strength) are reported as they provide useful mechanical information and could be convenient for comparisons between devices. The proposed test protocol was applied on 14 polypropylene meshes, 3 composite meshes, and 6 urogynecologic devices to verify its universal applicability towards meshes of different types and produced by various manufacturers, and its repeatability in terms of coefficient of variation.

The test protocol resulted easily applicable to all the tested surgical meshes with intra-subject variability characterized by coefficient of variations settled around 0.05. Its use within other laboratories could allow the determination of the inter-subject variability assessing its repeatability among users of alternative universal testing machines.

1. Introduction

Since the introduction of synthetic meshes for the strengthening of the abdominal wall in hernia repair surgery and for the treatment of pelvic organs prolapse, many studies tested commercial meshes in order to assess their mechanical characteristics (Deeken et al., 2011a; Hernández-gascón et al., 2011; Wolloscheck et al., 2004). The absence of specific standards to verify the safety and the performance of surgical meshes results in the arise of a plurality of test set ups, leading to dissimilar and often ambiguous methods used for the computation of mechanical parameters (Sahoo et al., 2015; Todros et al., 2017, 2018). Despite test methods (i.e., uniaxial, planar biaxial, equi-biaxial, ball burst, suture retention, and tear retention) have being repeated between studies, the variability between set ups and dimensions of the specimens makes the comparison between the results burdensome (Cordero et al., 2015; Deeken et al., 2011b, 2014; Wolf et al., 2013). In this context, the common practice is indeed to adapt, for the testing of surgical meshes (Deeken et al., 2011a), International Standards (ISs) or National Standards (NSs) originally developed for the textile industry as reported in Table 1. This adaptation is often induced by the limited availability of material linked to the small size and the high costs of the devices under investigation. Reductions in specimens dimension were indeed adopted by Li et al. (2014), Deeken et al. (2011b), Pott et al. (2012), whereas, for the same reason, a reduced number of replicas are performed by Maurer et al. (2014), that conducted only one or two replicas for each tested configuration. However, variability is found in other test parameters, such as the strain rate, for not always reported or justified reasons. In fact, despite the standards recommend values (e.g., ISs for ball burst test

* Corresponding author. Department of Mechanical and Aerospace Engineering, Politecnico di Torino, 10129, Turin, Italy.
E-mail address: vittoria.civilini@polito.it (V. Civilini).

https://doi.org/10.1016/j.jmbbm.2023.105987
Received 21 December 2022; Received in revised form 6 June 2023; Accepted 20 June 2023
Available online 20 June 2023

define a loading rate of 305 ± 13 mm/min) or ranges (e.g., ISs prescribe an elongation rate related to the gauge length - g.l. - of the specimen for uniaxial tensile tests and two elongation rates for the tear resistance test, to be selected in agreement with the manufacturer), strain rates reported in literature are widely variable. For instance, in uniaxial tensile test, strain rates greater than 100% g.l./min were used by Pott et al. (2012) (50 mm/min with a g.l. < 45 mm) and by Dietz et al. (2003) (1200 mm/min with a g.l. = 46 mm). On the contrary, Velayudhan et al. (2009) adopted a lower strain rate than the one suggested by the ASTM Standard followed (specimen used = 45x30, strain rate = 10 mm/min; ASTM specimen min g.l. = 75 ± 1 mm, strain rate = 300 ± 10 mm/min). Deviations about strain rate were also reported in ball burst test (Klosterhalfen et al., 2000). Moreover, various strain rates were selected in suture retention test, for which no reference standards are available (Deeken et al., 2011a; Klosterhalfen et al., 2000; Martin et al., 2013; Soares et al., 1996). An additional variation in ball burst set-ups regards the ratio between the clamped circle region and the sphere diameter (Deeken et al., 2011b; Klosterhalfen et al., 2000; Lerdsirisopon et al., 2011). Last, but not least, the post-processing of raw data is addressed with different methods in the literature. The aim of the post-processing is mainly the computation of the meshes mechanical properties. Some of these are described in the ISs, while many others can be defined and computed from experimental data in order to assess and compare the mechanical properties of the different surgical meshes. Some properties can indeed lead to a better understanding of implant acceptability (e.g., anisotropy, membranal tension, and strain), while others are useful for mechanical comparison (e.g., maximum uniaxial tensile force and tension, uniaxial stiffness) (Pott et al., 2012). Examples regarding differences in raw data manipulation can be found considering the stiffness of the specimens computed from the uniaxial tensile test data or the anisotropy between the two main directions of the knitted meshes. Regarding the stiffness, some studies used the slope of the secant at 10% of elongation (Maurer et al., 2014) or at 15% and 30% of elongation as high and low values, respectively (Jones et al., 2009; Moalli et al., 2008; Shepherd et al., 2012). Others calculate the slope of a small linear region of the stress-strain curves or load-displacement curves (Dietz et al., 2003; Li et al., 2014; Velayudhan et al., 2009) or in addition, consider the averaged slope of the whole linear portion of tension-strain curves (Saberski et al., 2011). On the contrary, Maurer et al. considers the ratio between the physiological membrane tension for the pelvic region calculated from Laplace's law (0.035 N/mm (Ozog et al., 2014)) and the corresponding $\Delta\varepsilon$ (Maurer et al., 2015). Finally, even though anisotropy is recognized as an important parameter for the correct graft alignment in order to minimize patient discomfort and recurrences (Anurov et al., 2012; Est et al., 2017; Rastegarpour et al., 2016; Zhu, 2015) it is rarely reported and, when done, different definitions are used (Deeken and Lake, 2017; Est et al., 2017; Maurer et al., 2014; Saberski et al., 2011).

The above-described issues impact the repeatability and reliability of the results and are the main cause of the meaningful variability reported in literature. Tables 1 and 2 collect the mechanical properties of polypropylene surgical meshes and urogynecologic devices (UD) focusing on the test types most frequently found in the literature: the ball burst test,

Table 1

Mechanical parameters of polypropylene and composite meshes (comp) reported in literature: BS: bursting strength; MTmax: maximum membrane tension; DSmax: maximum dilatational strain; DS16: dilatational strain at 16 N/cm; UTR: uniaxial tension at rupture; SR: strain at rupture; k: secant stiffness; SRS: suture retention strength. Column IS lists the standards cited in the study: a: ISO Standard - I: ISO 13934, II: ISO 527-1, b: ASTM standard - I: D3787-07, II: D638-03, III: D2261-07a, IV: D5034, c: National Standard - I: DIN 53455, II: DIN 54307, III: DIN 53857, d: Custom set up, NP not reported. The numerical values found in literature were converted for consistency with the units of measure used below. *1 replica performed; **2 replicas performed; ° value derived from bar graph; ^ sphere diameter equal to 9.53 mm.

				Ball Burst test				Uniaxial tensile test						Suture retention test	
				BS [N]	*MTmax* [N/cm]	*DSmax* [%]	*DS16* [%]	*UTR* [N/cm]		*SR* [%]		*k* [N/mm]		*SRS* [N]	
	Device	Reference	IS					Strong	Weak	Strong	Weak	Strong	Weak	Strong	Weak
LW	Bard™ Soft Mesh	Lerdsirisopon et al., 2011	b I		50.66 ± 2.42		12.03 ± 0.11								
	Parietene™	Pott et al., 2012	a I-II, c I					26.6 ± 4.2	38.9 ± 5.2	269 ± 10	294 ± 5	0.7 ± 0.1	0.9 ± 0.1		
	Prolene® Soft	Lerdsirisopon et al., 2011	b I		62.83 ± 2.14		14.40 ± 0.06								
	Ultrapro™	Maurer et al., 2014	d							43.9 ± 1.56**	35.1 ± 0.57**	0.1**	0.3**		
		Pott et al., 2012	a I-II, c I					6 ± 8.2	100.9 ± 9.4	187 ± 33	195 ± 5	0.3 ± 0.3	4.6 ± 0.5		
		Eliason et al., 2011	b I		35.5 ± 1.7		16.2 ±0.1								
		Saberski et al., 2011	d									0.87	10.21		
	ProLite Ultra ™	Deeken et al., 2011b	b I-II-III		50.72 ± 3.20		16.35 ± 0.19	19.11 ± 3.98.	44.46 ± 2.77					23.89 ± 3.4	36.07 ± 1.6
	Proceed® (Prolene Soft Mesh + ORC)	Eliason et al., 2011	b I		52.6 ± 5.1		7.3 ± 0.3								
SW	Bard™ Mesh	Deeken et al., 2011b	b I-II-III		157.70 ± 7.98		10.76 ± 0.18	1.17 ± 0.15	84.97 ± 12.26					66.80 ± 4.2	50.78 ± 2.1
		Martin et al., 2013	d	302.48^										35.59	
		Maurer et al., 2014	d							44.9*	30.9*	1*	2.9*		
	Prolene®	Deeken et al., 2011b	b I-II-III		156.60 ± 9.23		5.27 ± 0.07	4.02 ± 1.06	85.12 ± 7.63					61.20 ± 2.1	70.49 ± 2.6
		Li et al., 2014	d					72.23	92.75	134	78	1.04	5.99		
		Pott et al., 2012	a I-II, c I					41.6 ± 5.4	84.8 ± 15	274 ± 6	186 ± 7	1.1 ± 0.1	3.6 ± 0.4		
		Klosterhalfen et al., 2000	c II-III, d	2369	90	44	7	119.4	153.4					57	74.6
		Wolloscheck et al., 2004	d					4.6	15.07						
		Soares et al., 1996	d									7.8 - 12.35 °	11.7 - 15.6 °	51.5 ± 8.9	51.3 ± 6.6
		Klosterhalfen et al., 2005	NP				6							116	145
		Junge et al., 2001	c II				6.9 °								
		Velayudhan et al., 2009	b IV									1.8-2.2 °	5.5-6.5 °		
		Dietz et al., 2003	d					51.27 ± 7.38				0.53 ± 0.15			
	ProLite ™	Deeken et al., 2011b	b I-II-III		138 ± 2.27		9.61 ± 0.19	0.75 ± 0.09	54.71 ± 7.90					57.71 ± 1.9	48.75 ± 3.0
		Saberski et al., 2011	d									2.54	5.99		
	DynaMesh® ENDOLAP	Maurer et al., 2014	d							40.85 ± 2.76**	40.1*	0.25 ± 0.07**	0.3*		
	Surgipro™ PP Monofilament Mesh	Maurer et al., 2014	d							40.9*	33.6 ± 1.27**	2.5*	2.55 ± 0.21**		
		Pott et al., 2012	a I-II, c I					38.6 ± 12.3	46.5 ± 4.1	213 ± 13	228 ± 4	1.3 ± 0.3	1.4 ± 0.1		
	Trelex®	Saberski et al., 2011	d									3.31	7.69		
Comp	Composix™ L/P	Deeken et al., 2011a	b I-II-III		76.77 ± 3.68		11.06 ± 0.54	10.21 ± 0.90	42.09 ± 1.86					48.58 ± 1.3	34.04 ± 1.8
	Composix™ E/X	Deeken et al., 2011a	b I-II-III		237.80 ± 10.49		9.62 ± 0.58	12.82 ± 2.05	95.59 ± 9.88					70.47 ± 4.4	60.28 ± 2.4
	Dynamesh - IPOM ® (PVDF + PP)	Pott et al., 2012	a I-II, c I					11.1 ± 6.4	46.9 ± 9.7	340 ± 20	193 ± 8	0.3 ± 0.1	1.9 ± 0.4		

the uniaxial tensile test, and the suture retention test. Synthetic meshes were classified by density: ultra-light weight (ULW), light weight (LW), standard weight (SW) and heavy weight (HW) (Coda et al., 2012). In addition to the dispersion of the data, the incompleteness of the table stands out, representing the lack of multi-test protocols that the authors can follow to mechanically characterize the devices.

In this panorama, the aim of this study is to propose a comprehensive test protocol comprising: (1) a set of mechanical testing methods adapted from the ISs and (2) the post-processing algorithms used to extract from the raw data the mechanical parameters useful to compare different devices. The defined test protocol is tested on 23 different devices to confirm its repeatability on devices having different structures and different intended use.

2. Materials and methods

Three quasi-static test methods were selected with the aim of providing the parameters of interest albeit using tests characterized by ease of execution and adaptability in terms of specimens dimensions. In detail, given its multiaxial characteristic, the static ball burst test was selected for performance assessment. It indeed replicates a solicitation pattern that resembles the *in vivo* load state, and it can therefore be used to evaluate rupture behavior at high loads and deformability behavior under physiological or pathological stresses. The static uniaxial test is the most performed mechanical test and was therefore selected to provide basic mechanical characteristics. A static suture retention test was added to complete the surgical meshes mechanical characterization providing parameters related to the mesh positioning procedure. In order to evaluate different behaviors along the two principal direction of the knitted pattern of the meshes, specimens were collected in two perpendicular directions mention as “weak” and “strong” in the paragraphs below. The “strong” direction was determined comparing the failure force obtained in the uniaxial tensile test by the specimens of the same mesh in the two directions. The three set ups are shown in Fig. 1.

2.1. Ball burst test protocol

ASTM D6797-15 is used as reference standard for this test. Reduced circular specimens (diameter = 55 mm) and ball-burst attachment dimensions (ring clamp internal diameter (aperture) = 35 mm and polished steel sphere diameter = 20 mm) are used in place of the recommended ones in order to allow testing and comparison between surgical meshes of small and variable commercial sizes. The ratio between the aperture and the ball diameter suggested by the standard (44.45 mm/25.4 mm = 1.75) is not modified.

A custom test grasping based on a screw mechanism was realized in INOX AISI 316, in order to apply a uniform pressure on the constrained annulus of the specimen allowing to clamp the specimens without tension between the plates of the ring clamp mechanism (Fig. 1a, the .STEP file of the ball burst grasping mechanism is provided in the Supplementary Material).

After specimen positioning, the spherical indenter is moved towards the mesh at 300 mm/min as the standard prescribes, while recording the force and the displacement. For each mesh typology, five specimens are tested as suggested by the standard, in order to give statistical consistency of results.

2.1.1. Parameters computation

From the raw data the bursting strength is computed as the maximum force value. Due to the dependency of the maximum force on the ratio between the sphere diameter and the aperture diameter, the computation of membrane tension and strain is also mandatory for comparison purposes. These parameters are computed through an analytical method developed by Freytes et al. (2005) and Sahoo et al. (2015), which relies on the following assumptions:

- The specimen is isotropic, incompressible, there are negligible shear stress, and negligible friction between the steel ball and the specimen;
- The specimen can be modeled as a thin-walled membrane (i.e., specimen thickness is negligible, being more than one order of magnitude lower than specimen radius).

The method is briefly described below for ease of reference.

During the test, the ball-specimen contact area progressively increases and the ball traversing the specimen leads to specimen deformation that assumes the shape shown in Fig. 2a. Therefore, the central region of contact assumes a spherical dome shape, while the peripheral region, out of contact, assumes a truncated cone shape, with a base equal to the fixed-edge of the aperture (Fig. 2b).

The dilatational strain (*DS*, %) is defined as the percent modification of specimen area as the ball penetrates the specimen:

$$DS = \frac{A_i - A_0}{A_0} 100\% \quad [1]$$

where the initial specimen area is $A_0 = \pi a^2 = 962.11\ mm^2$.

The instantaneous specimen area A_i at each time step i can be calculated as the sum of the surface area in contact with the ball, A_b and the truncated cone area, A_c. The estimation of the two areas needs the computation of geometric entities starting from the ball displacement l recorded by test machine ([mm]), the ball radius R and the aperture radius a as follows:

- The distance b between the aperture and the ball centroid is calculated as $b = R - l$ for $l < R$ or $b = l - R$ for $l > R$ (Fig. 2c and d).
- The free length of the specimen is computed as $f = \sqrt{a^2 + b^2 - R^2}$ (derived from $c^2 = f^2 + R^2 = a^2 + b^2$).
- The angle φ between the vertical axis and the line connecting ball centroid and the boundary point between the contact with the ball and the free length of the specimen (point A in Fig. 2b and c) is computed as $\varphi = \tan^{-1}\left(\frac{a}{b}\right) - \tan^{-1}\left(\frac{f}{D}\right)$ if $l < R$ and as $\varphi = \pi - \tan^{-1}\left(\frac{a}{b}\right) - \tan^{-1}\left(\frac{f}{R}\right)$ if $l > R$.
- Therefore:
  - A_b is computed by integration of the dome circumference along the angle ε (in red in Fig. 2c) which spans from 0 to φ: $A_b = \int_0^{\varphi} 2\pi \bullet R \sin\varepsilon \bullet R\, d\varepsilon = 2\pi R^2[1 - \cos\varphi]$;.
  - A_c is directly computed from geometric relations as $A_c = \pi f(r_b + a)$.
- Finally, $A_i = A_b + A_c$.

The true membrane tension depends on the instantaneous specimen-edge length and the corresponding load, which is generated by the pressure applied to the specimen through the ball during the test. The true membrane tension depends on the radius in the truncated cone portion of the specimen free from the ball, decreasing as the considered radius increases. The maximum solicitations are therefore gathered at the r_b radius, while solicitations decrease approaching the aperture. For this reason, both membrane tensions are computed (at $r = r_b$ and $r = a$).

The pressure P acts on the contact region, defined in Fig. 2a, called A_b in the previous section, and it is estimated from thin membrane theory as:

$$P = \frac{L}{A_b} = \frac{L}{2\pi R^2[1 - \cos\varphi]} \quad [2]$$

It follows that the true membrane tension (T, N/cm) in the specimen contact area ($r = r_b$) can be estimated as:

$$T = \frac{PR}{2} = \frac{L}{2\pi R^2[1 - \cos\varphi]} \bullet \frac{R}{2} = \frac{L}{4\pi R[1 - \cos\varphi]} \quad [3]$$

The true membrane tension at the aperture ($r = a$, see Fig. 2d) is

Table 2
Mechanical parameters of polypropylene urogynecologic devices reported in literature: UTR: uniaxial tension at rupture; SR: strain at rupture; k: secant stiffness. No International Standard are reported in literature for urogynecologic devices. The numerical values found in literature were converted for consistency with the units of measure used below. *1 replica performed; **2 replicas performed.

			Uniaxial tensile test					
			UTR [N/cm]		*SR* [%]		*k* [N/mm]	
	Device	Reference	Strong	Weak	Strong	Weak	Strong	Weak
ULW	Gynecare Ultrapro™ as Prolift + M™ (PP+Polyglecaprone)	Shepherd et al., 2012	5.22 ± 0.47		87.9 ± 5.6		low stiffness 0.009 ± 0.00; high stiffness 0.236 ± 0.02	
	Smartmesh™ as Restorelle™	Maurer et al., 2014			33 ± 7.64**	33 ± 7.64**	2.55 ± 0.07**	2.55 ± 0.07**
	Smartmesh™ as Minimesh™	Shepherd et al., 2012	22.7 ± 1.8		68.5 ± 2.5		low stiffness 0.178 ± 0.03; high stiffness 0.592 ± 0.04	
	IntePro Lite™ as Elevate™	Shepherd et al., 2012	18.13 ± 1.27		67.6 ± 2.1		low stiffness 0.071 ± 0.01; high stiffness 0.934 ± 0.04	
	NovaSilk™	Shepherd et al., 2012	13.07 ± 3		89.4 ± 21.4		low stiffness 0.072 ± 0.05; high stiffness 0.508 ± 0.09	
	Pelvitex™	Jones et al., 2009	11.07 ± 1.40		100.65 ± 8.62		low stiffness 0.07 ± 0.03; high stiffness 0.87 ± 0.07	
	Popmesh™	Jones et al., 2009	4.28 ± 1.23		60.95 ± 9.96		low stiffness N/A; high stiffness 0.36 ± 0.09	
LW	Parietex Ugytex®	Maurer et al., 2014			40.1 ± 0.85**	40.1 *	2.6 ± 0.57**	5.1*
	Polyform™	Shepherd et al., 2012	35.86 ± 3.2		86.5 ± 2.4		low stiffness 0.130 ± 0.01; high stiffness 1.42 ± 0.11	
		Jones et al., 2009	10.33 ± 1.71		92.25 ± 16.70		low stiffness 0.05 ± 0.01; high stiffness 0.69 ± 0.13	
	Timesh™	Jones et al., 2009	1.92 ± 0.24		61.66 ± 4.52		low stiffness 0.02 ± 0.01; high stiffness 0.17 ± 0.03	
SW	Gynecare TVT™	Dietz et al., 2003	61.90 ± 23.45				0.23 ± 0.05	
		Moalli et al., 2008	73.5 ± 11.8		108.1 ± 4.5		low stiffness 0.09 ± 0.01; high stiffness 2.0 ± 0.3	
	Gynecare Gynemesh PS™ as Prolift™ (Prolene Soft Mesh)	Shepherd et al., 2012	30.87 ± 1.73		66.7 ± 4.6		low stiffness 0.286 ± 0.02; high stiffness 1.37 ± 0.09	
		Jones et al., 2009	13.67 ± 2.49		71.50 ± 2.97		low stiffness 0.27 ± 0.09; high stiffness 1.25 ± 0.21	
		Maurer et al., 2014			59.65 ± 12.54**	40.3 ± 2.40**	0.65 ± 0.21**	2.35 ± 0.07**
	DynaMesh® PRS	Maurer et al., 2014			31.8 ± 7.21**	21.9*	1.85 ± 0.21**	14.7*
	Sparc Tape	Dietz et al., 2003	47.36 ± 13.64				0.53 ± 0.15	
	IVS Tape	Dietz et al., 2003	57.75 ± 5.25				1.58 ± 0.31	

estimated as:

$$T_a = T \times \frac{2\pi r_b}{2\pi a} = T \times \frac{R \sin \varphi}{a} \quad [4]$$

The true tension in the portion of the mesh in contact with the sphere, T, is the greatest tension that the specimen stands and is therefore used to compute the maximum membrane tension and the corresponding dilatational strain. On the other hand, the true membrane tension at the aperture, T_a, is the tension that affects the entire area of the specimen and can be thus considered to assess the dilatational strain of the graft corresponding to a membrane tension of 16 N/cm and at 32 N/cm, that corresponds to the most reported tension requirements for surgical meshes (Bilsel and Abci, 2012; Deeken et al., 2011a; Zhu, 2015).

2.2. Uniaxial tensile test protocol

Test parameters are selected with reference to the ISO 13934-1:2013 international standard. Being the reference standard not designed for medical device testing, a change in specimen shape and dimension was necessary in order to allow testing and comparison between meshes of small and variable commercial sizes. The actual specimen design (Fig. 1b, the 2D drawing of the dogbone specimen is provided in the Supplementary Material) was obtained through an iterative experimental process aimed at avoiding specimens rupture within 5 mm from the grip (jaw break), as prescribed by the standard. Indeed, according to the standard, these specimens need to be discarded from subsequent evaluations.

Due to the choice of dogbone specimens and, at the same time, the impossibility to attach a strain gauge to the specimen because of material nature, it is necessary to use an optical measurement system in order to analyze the displacement of the necking zone of the specimen. Therefore, two markers are sewn on the mesh, in the narrow section, taking care not to interfere with the movement between the yarns. The initial distance between the markers is 20 mm. Markers displacements are recorded and analyzed using a Digital Image Correlation (DIC) system after the cameras calibration.

Five specimens for the two principal knitting direction of each mesh types are tested. The specimens are mounted on the testing machine by the mean of pneumatic grips set to 1.8 bar without a preload, and the upper grip is moved vertically at 20 mm/min, 100% gauge length/min

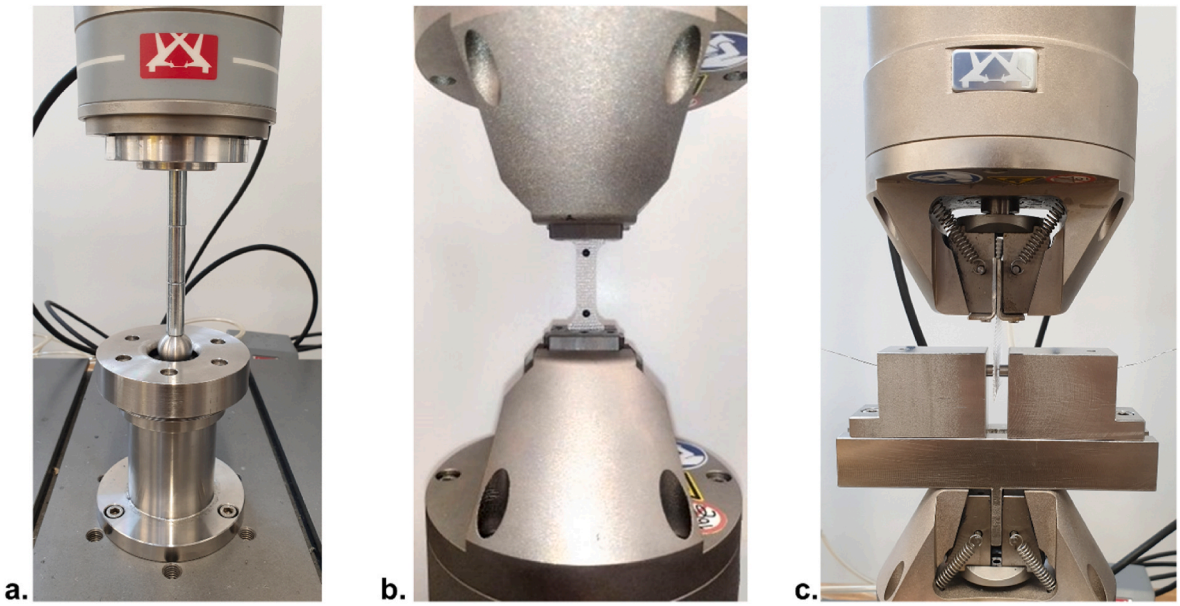

Fig. 1. Tests set up with an example of a mounted specimen. a) Ball burst test; b) Uniaxial tensile test; c) Suture retention test.

elongation rate as suggested by the standard for specimens that exhibit elongation at maximum force of fabric >75%. The force and the displacement data as well as images are acquired at 5 Hz.

2.2.1. Parameters computation

From marker coordinates, the deformation in the central portion of the specimen is computed as:

$$\varepsilon = \frac{l - l_0}{l_0} * 100 \quad [5]$$

where l is the incremental marker distance along the motion axis, and l_0 is the initial marker distance at rest along the motion axis.

From the force F recorded during the test, the tension is computed as:

$$T = \frac{F}{w_0} \quad [6]$$

where w_0 is the specimen width at rest, equal to 8 mm in the dogbone geometry defined.

The tension at rupture and the corresponding strain are reported as meaningful parameters. From the tension vs. deformation curve, the slope of the initial portion, named secant stiffness (k), is computed as the slope of secant line at 10% deformation (Maurer et al., 2014). This value of strain is considered as representative of a physiological range of deformation for implanted devices (Junge et al., 2001; Konerding et al., 2011; Ruiz-zapata et al., 2018). A representative tension vs. strain curve is shown in Fig. 3 depicting the computed parameters.

The anisotropy of the meshes is thus computed starting from the mean value of secant stiffness in the two perpendicular directions as:

$$\alpha = \left| \log \frac{k_s}{k_w} \right| \quad [7]$$

where k_s is the secant stiffness in the strong direction and k_w in the weak direction (Saberski et al., 2011).

2.3. Suture retention test protocol

The attachment and the test setup, showed in Fig. 1c, were designed, adapting the setup used by Deeken et al. (2011b), and were realized in INOX AISI 304 (the .STEP file of the suture retention test grasping mechanism is provided in the Supplementary Material). Rectangular specimens (70 x 55 mm) are securely clamped without tension at the upper pneumatic grip set to 1.8 bar, while a Assusteel® monofilament wire with a diameter of 0.350–0.399 mm is inserted 10 mm from the inferior edge of each specimen. The specimens are loaded at a rate of 300 mm/min in displacement control and the force and the displacement data are acquired. Five specimens for the two principal knitting direction of each mesh types are tested.

2.3.1. Parameters computation

From the raw data, the suture retention strength (F_{max}) for the single specimen is computed as prescribed by the ASTM D2261-13 (Fig. 4):

- Option 1: For fabrics exhibiting five peaks or more, after the initial peak, determine the five highest peak forces and calculate the average of these five highest peak forces.
- Option 2: For fabrics exhibiting less than five peaks, record the highest peak force as the single-peak force.

2.4. Test protocol verification

Fourteen polypropylene meshes, used for abdominal or inguinal hernia repair, three composite meshes used for abdominal hernia repair and six urogynecologic devices, used for pelvic floor disorders (i.e., pelvic organ prolapses and stress urinary incontinence), were tested in the three different set ups in order to verify its suitability for the surgical meshes. Only the uniaxial tensile test in longitudinal direction was conducted on the urogynecologic devices.

All the tests were performed using a universal testing machine, Instron E3000 (INSTRON®, Norwood, MA, USA) under displacement control conditions. The sensors used to record the force and the displacement during the tests are certified with an Accuracy Class 0.5 specify in ISO 9513:2012. The requirements of the aforementioned IS (e.g., ISO 13934-1:2013 and ASTM D6797-15) are therefore completely fulfill. The VIC-3D system (Isi-sys GmbH, Kassel, Germany) was used to record the markers displacement during uniaxial tests. The post-processing of the data was entirely conducted in Matlab (version 9.10.0 (R2021a). Natick, Massachusetts: The MathWorks Inc.).

Due to the devices dimensions, it was not possible to carry out all test methods for all the selected meshes. The tests performed on each mesh (335 specimens in total) are indeed detailed in Table 3 where the devices are grouped by intended use as hernia meshes (HM) and urogynecologic

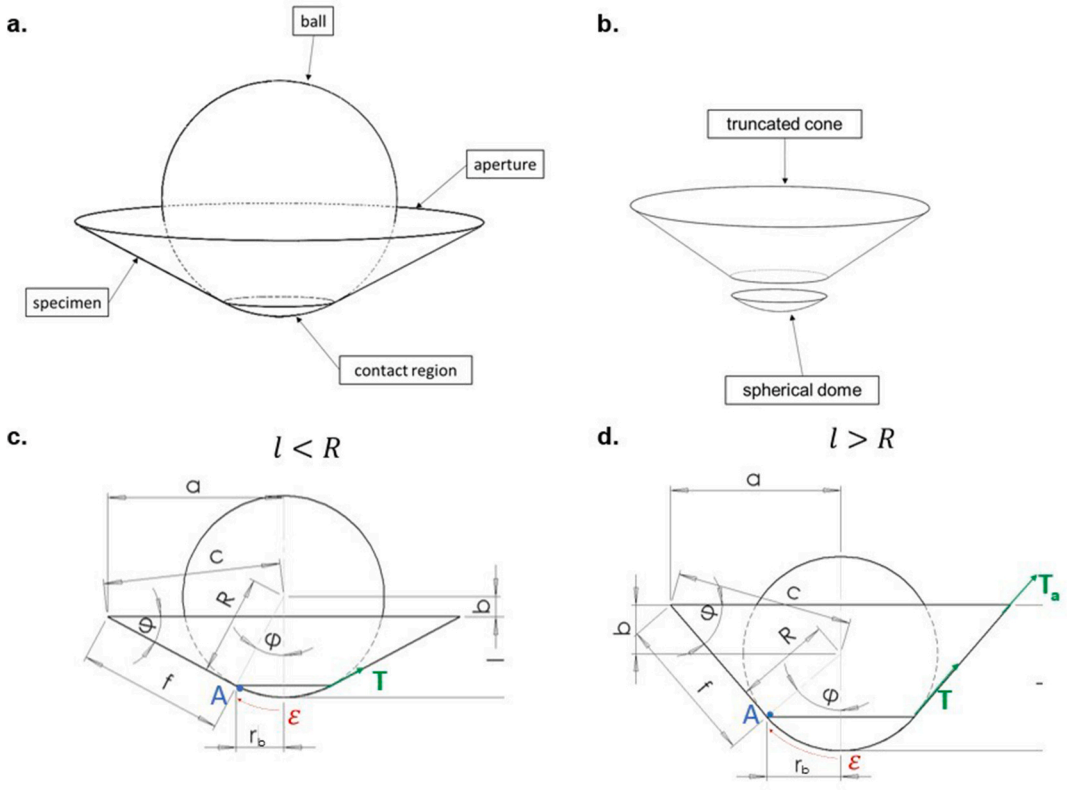

Fig. 2. Schematic of the ball-burst test setup: a) representation of the ball-sample contact; b) split of the specimen geometry into a spherical dome and a truncated cone; c-d) geometrical parameters used in estimating mechanical properties of the test construct when the ball displacement is lower than the radius of the ball (c) and when the ball displacement is higher than the radius of the ball (d).

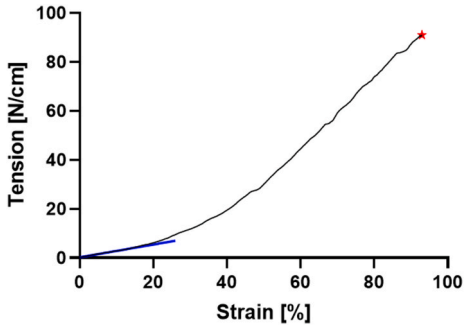

Fig. 3. Representative tension vs. strain curve for uniaxial tension test. The blue line represents the secant stiffness computed as detailed above, whereas the red star depicts the tension at rupture and the corresponding strain.

devices (UD) and by weight in ultra-light weight (ULW), light weight (LW), standard weight (SW) and heavy weight (HW) or composite (Comp), as previously described.

In order to determine the dispersion level around the mean and to verify the test protocol repeatability, the coefficient of variation (CV) was determined for all the extracted parameters, with the exception of anisotropy, as the ratio between the standard deviation and the mean computed on the 5 replicas performed for each tested configuration. Moreover, the median value of the CV was assessed for each set up gathering the CV values of the different parameters computed from the raw data.

3. Results

For each tested configuration five replicas were performed. The repeatability of the test was evaluated by the mean of frequency analyses on the CVs.

The first frequency analysis was implemented between the CVs of all the parameters and all the devices for each test method. The results are displayed in Fig. 5 as bar diagrams and heat maps. The bar diagrams depict the CVs values of all the parameters computed for each test method. The heat maps draw the attention on the CVs distribution of the different parameters. Considering the three test types, the CVs distribution is highly concentrated in a range between 0.05 and 0.20, as highlighted by the darker colors of the heat map above 0.20. The median values of CVs for the different tests are: 0.14 for the uniaxial tensile test, 0.05 for the ball burst test, and 0.08 for the suture retention test.

Additionally, the frequency distribution of CVs for all the parameters of all the test methods is shown in Fig. 6 toghether with the frequency distribution of the CVs of the parameters found in literature and reported in Tables 1 and 2. Among all the tests parameters the most frequent CV value is 0.05. The frequency distribution appears similar comparing our parameters to literature parameters. However, in literature there are sporadic CVs equal or higher than 1 wheres CVs higher then 0.30 are rare in our results.

The repeatability of the test is reflected in the standard deviations of the force-displacement curves, that are usually limited in comparison to the respective mean value. Some examples are shown in Fig. 7, Figs. 8 and 9 in which the low variability is observable in the depicted curves, where the standard deviation is represented as a semi-transparent area around the mean. Herein, the curves are reported only to further stress the repeatability of the performed tests. In this regard, the names of the meshes were not disclosed to prevent the attention from shifting towards the comparison of meshes and manufacturers, which falls beyond the

Table 3
Tested meshes for the three test methods.

		Mesh ID	Ball Burst Test	Uniaxial Tensile Test		Suture Retention Test	
				Weak	Strong	Weak	Strong
HM	LW	1	●	●	●	●	●
		2	●	●	●	●	●
		3	●	●	●	●	●
		4	●	●	●	●	●
		5	●	●	●	●	●
		6	●	●	●	●	●
	SW	7	●	●	●	●	●
		8	●	●	●	●	●
		9	●	●	●	●	●
		10	●	●	●	●	●
	HW	11		●	●		
		12		●	●		
		13		●	●		
		14		●	●		
	Comp	15	●				
		16	●				
		17	●				
UD	ULW	18		●			
	LW	19		●			
		20		●			
	SW	21		●			
		22		●			
		23		●			

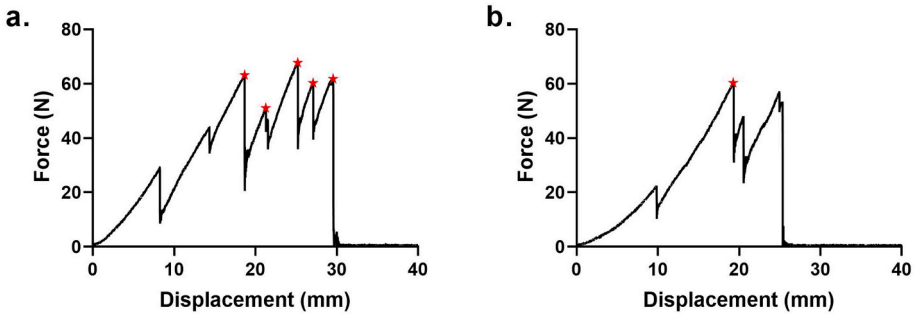

Fig. 4. a) Representative force vs. displacement curve for option 1 peaks detection; b) Representative force vs. displacement curve for option 2 peaks detection.

scope of the work presented here.

From the ball burst curves (Fig. 7) almost identical trends are appreciable in all LW meshes that exhibit overlapped areas. Similar trends are displayed also from SW meshes. In this case, the main differences are in terms of maximum reached displacement. The composite meshes also reveal trends shifted in terms of displacement. From Fig. 8 differences between the two tested directions can be stressed out. In particular, the anisotropy appears to be higher for the HW meshes with the exception of mesh 4 that reaches the highest anisotropy value. Only three meshes (i.e., mesh ID 2, 3 and 10) show similar behavior in the two tested directions with an anisotropy value less than 0.10. The HW meshes have completely separated curves between the two directions, with a high overlap among the devices mostly in the strong direction. The urogynecologic devices (Fig. 9) can be grouped in three couples with similar behavior, especially in terms of stiffness. Moreover, greater strains at rupture values are obtained from the urogynecologic devices with lower secant stiffness.

A comparison between the computed parameters for all the 23 meshes is conducted in order to assess a correspondence between the mechanical parameters and the types of meshes. The most relevant parameters are depicted in Fig. 10. Here, BF and SRS appear the most suitable mechanical parameters for a classification of the meshes showing a clear separation between the LW and the SW meshes. The composite meshes results in the BF graph are similar to the LW meshes,

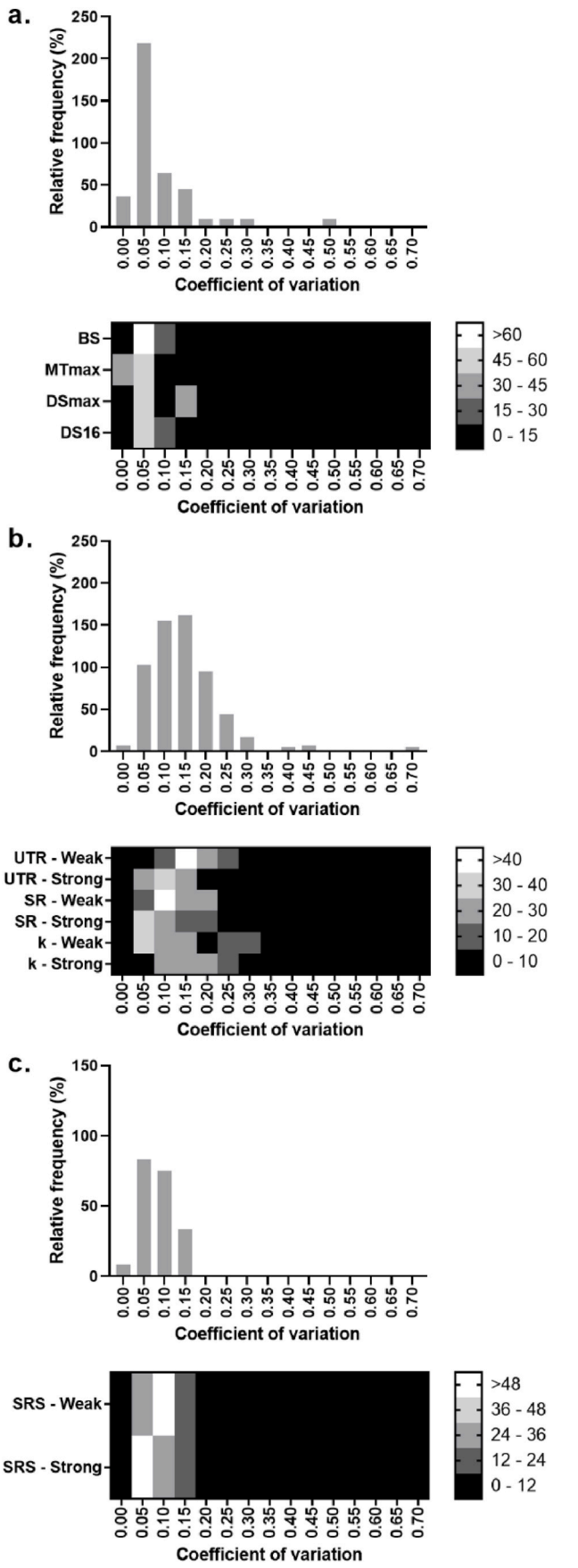

(caption on next column)

Fig. 5. CVs frequency analysis among all the parameters for the selected test method. a) Ball Burst test where BS: bursting strength; MTmax: maximum membrane tension; DSmax: maximum dilatational strain; DS16: dilatational strain at 16 N/cm; DS32: dilatational strain at 32 N/cm; b) Uniaxial tensile test where UTR: uniaxial tension at rupture; SR: strain at rupture; k: secant stiffness; c) Suture retention test where SRS: suture retention strength. The color percentage near the heat maps refers to the relative frequency percentage of the corresponding CV value.

as composite devices, here tested, are made up of a layer of different LW meshes and a non-adhesion membrane layer that does not significantly improve the mechanical properties of the devices. Finally, about uniaxial tensile test, a grouping of the different meshes weights is possible by combining information from UTR and k results. In detail, LW meshes differentiate from SW and HW thanks to UTR values, whereas HW meshes obtained higher k values in the strong direction comparing to the SW meshes.

4. Discussion

The adoption of ISs used worldwide to assess the mechanical characteristic of surgical meshes would be a chance to reduce the variability of tests set ups and methods for parameters computation, making the comparisons between different studies more reliable, or at least possible. In this perspective, the present study proposes an exhaustive test protocol for the mechanical characterization of synthetic meshes. The test protocol consists of a ball burst test, a uniaxial tensile test and a suture retention test. For the ball burst test, a steel sphere with a 20 mm diameter was used to penetrate a circular specimen with an indentable diameter of 35 mm. The sphere was moved along the vertical direction at a strain rate of 300 mm/min. In the uniaxial tensile test, a dogbone specimen with a gauge length of 20 mm was tensioned at a strain rate of 20 mm/min until rupture. Finally, in suture retention test a 70 x 55 mm rectangular specimen was tested, propagating the threads rupture caused by an Assusteel® wire inserted 10 mm from the bottom edge of the specimen. The test was performed at a strain rate of 300 mm/min.

Our set up choices were driven mainly by the prospect to easily replicate the tests (i.e., small specimens, simple set ups and, detailed computation of parameters), without neglecting the possibility of comparison with physiological conditions.

We at first addressed the reduction of the specimens dimensions to limit the material needed for the tests. In this regard, if the scarcity of material, especially in specimens collected from preshaped devices (i.e., heavy weight and composite meshes), precludes the performance of all tests, we recommend excluding the suture retention test on those meshes. In our opinion, the uniaxial tensile tests and the ball burst test are the most significant for the comparison of the mechanical properties of surgical meshes. The need in performing at least uniaxial tensile test and ball burst test rises from the complex mechanical behavior of these textile implantable devices and moreover, the complex solicitations pattern that they have to stand once implanted.

The reduction of specimen dimensions for the uniaxial tensile test was crucial, as the prescription of the most used IS (i.e., ISO 13934) declares a rectangular specimen with a width of 50 mm and a gauge length of 200 mm (100 mm for material with an elongation greater than 75% of g.l.). These sizes may be acceptable in the analysis of general fabrics but become inapplicable in the case of surgical meshes. The process followed in order to determine the best compromise in terms of small dimensions and failure in the central part of the specimen led to the selection of a dogbone shape, which however made the use of an optical system mandatory to follow and acquire the displacement of the narrow part of the specimen. In many studies that perform uniaxial tensile tests on dogbone specimens, there is no mention to local measurements, neither with optical methods nor other techniques, for the recording of the actual displacement of the narrowed section of the

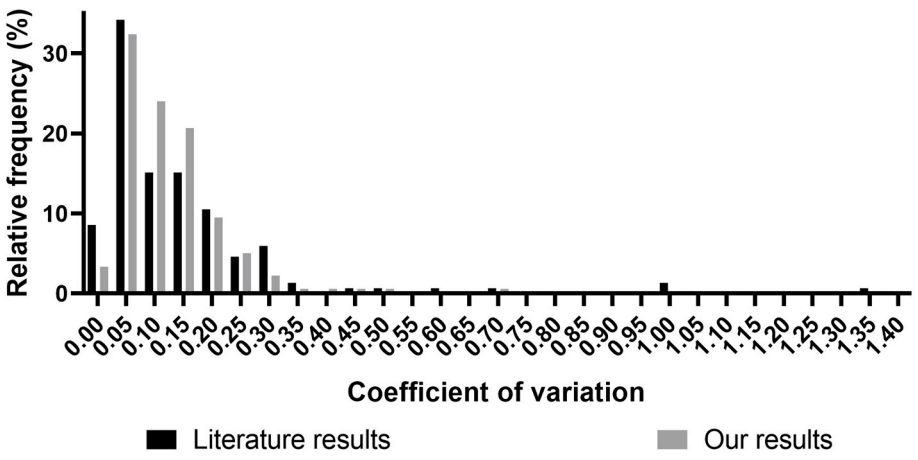

Fig. 6. Frequency analysis of CVs among all the tests parameters reported in literature.

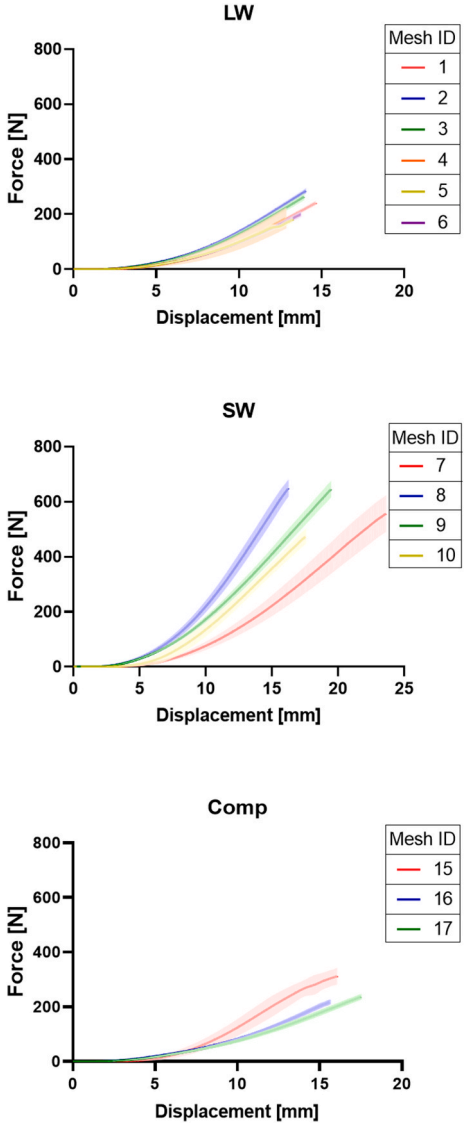

Fig. 7. Force vs displacement curves from ball burst test data. The lines depict the mean behavior obtained from the five replicas whereas the standard deviation is represented as semi-transparent area around the mean. In each graph, different colors refer to different devices and the numbers in the legend refer to Table 3.

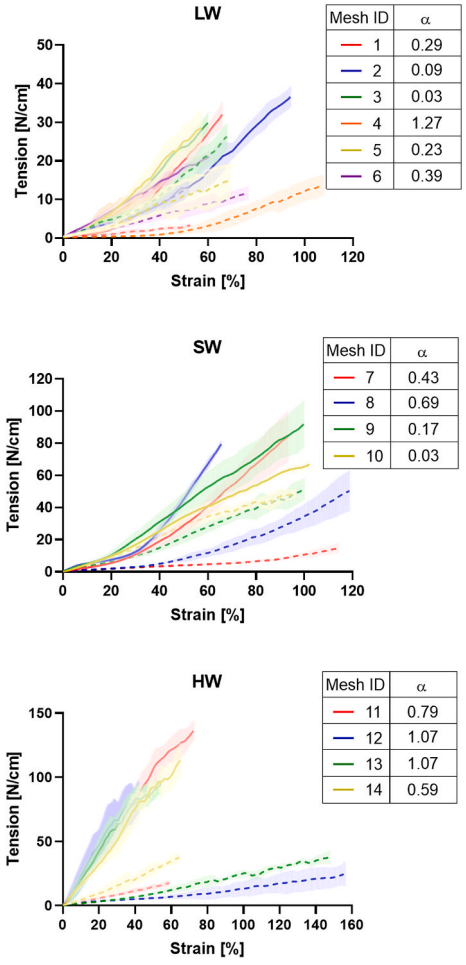

Fig. 8. Tension vs. strain curves from uniaxial tensile test data of hernia mesh. The lines depict the mean behavior obtained from the five replicas whereas the standard deviation is represented as semi-transparent area around the mean. In each graph, different colors refer to different devices and the numbers in the legend (tables on the right of graphs) refer to Table 3. The dashed lines refer to the weak direction, while the solid lines refer to the strong direction. The tables on the right report the anisotropy value for each mesh.

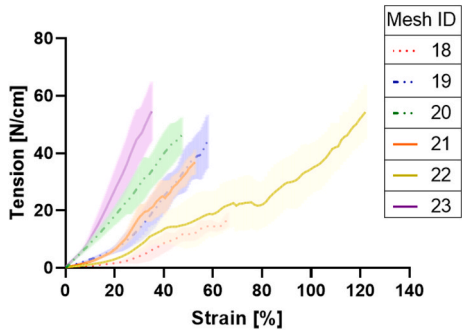

Fig. 9. Tension vs. strain curves from uniaxial tensile test data of urogynecologic devices. The lines depict the mean behavior obtained from the five replicas whereas the standard deviation is represented as semi-transparent area around the mean. Different colors refer to different devices and the numbers in the legend refer to Table 3. The solid lines refer to the SW devices, the dashed and dotted line to the LW device and the dotted line to the ULW device.

specimen (Deeken et al., 2011b; Li et al., 2014; Pott et al., 2012). The use of the displacement recorded by the testing machine when dealing with dogbone specimens leads to a wrong estimation of mechanical parameters, due to the non-constant cross-section of the specimen. A local strain measure is therefore mandatory to compare the stiffness and strain results using the proposed test protocol. Regarding the computed parameters, the choice of a small width could have affected results especially for the lighter meshes in which the large porosity leads to a small amount of load-bearing threads (Pott et al., 2012). Moreover, not all the tested meshes attained a 75% elongation at rupture that is reported by the IS for the use of a strain rate equal to 100% of gauge length/min. Still, the strain rate was not varied between the different materials both considering that the majority of the surgical meshes reached the required elongation at rupture, and to allow comparability between the results.

In ball burst test, the bursting strength is highly dependent on the aperture and the sphere diameters, and, as a consequence, on the circular specimen diameter. Nonetheless, the membrane tension and the dilatational strain depend only on the ratio between the two diameters. Changes in the specimens dimensions is therefore possible as long as the ratio between the aperture and the sphere diameter remains unchanged (1.75 as suggested by ASTM D6797-15 standard).

In the proposed protocol the wider specimens are needed in the suture retention test, because smaller specimen dimensions always resulted in an incorrect and transverse propagation of the tear. Not only the size but also the Assusteel wire distance from the specimen edge affects the suture retention strength: a change in this distance would vary the number of mesh threads that withstand to the tear propagation and so the number and the value of force peaks.

Although the parameters used to compare mesh performance recur in literature, the computation of these parameters is often not clearly described (e.g., tensile stress and strain in Deeken et al., 2011b and Eliason et al., 2011 for ball burst test) making the results interpretation troublesome. By providing a detailed description of how to calculate the mechanical parameters which we consider to be of interest, we encourage the use of directly comparable results. In this way an inter-subject variability analysis could be easily conducted in order to settle the strongest parameters by computing CVs for a same parameter collected in different laboratories.

A further issue for mechanical parameters extracted by *in vitro* test is their correlation with clinical outcomes and some studies emphasize the importance of mechanical parameters in order to get information of *in vivo* behavior or at least to guide the surgeon's choice of feasible device (De Maria et al., 2016; Hollinsky et al., 2008; Klinge and Klosterhalfen, 2012). On the other hand, other studies highlight that, at present, no simple correlation was found between biomechanical parameters and clinical outcomes, especially using uniaxial tests (Mangera et al., 2012; Maurer et al., 2014). Therefore, many precautions should be taken in interpreting the parameters extracted from *in vitro* tests. Moreover, the definition of mechanical requisites for the surgical meshes could be much more laborious due to the difficulties in the assessment of the physiological stress and strain state. The actual tension and the corresponding deformation that act on abdominal wall, inguinal canal and

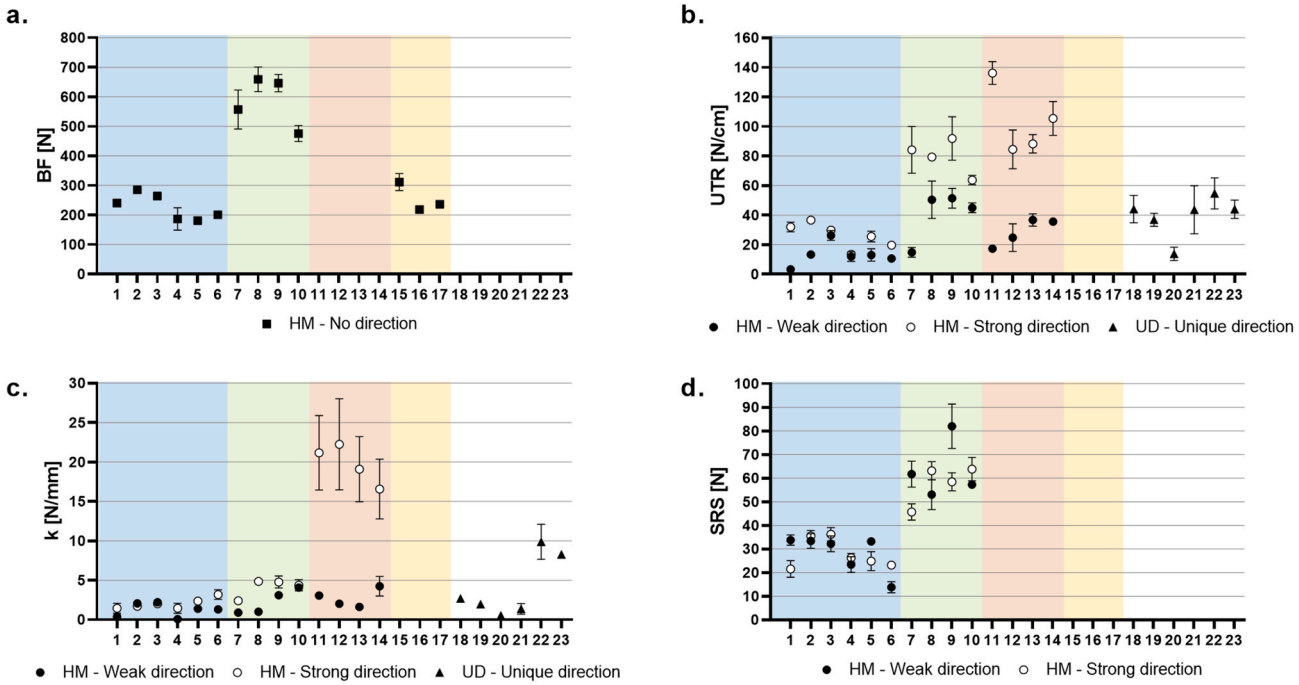

Fig. 10. Mechanical parameters computed for the tested meshes relevant for devices classification: a) BF computed from ball burst test for HM, b) e c) UTR and k respectively, computed from uniaxial tensile test and d) STS computed from suture retention test. The colored bands delimited the different meshes weight for HM: blue band for the LW, green band for the SW, orange band for the HW, yellow band for the Comp and finally violet dotted band for all the UD.

pelvic floor during everyday activities has been investigated by the mean of different approach but are still relatively not defined (Cobb et al., 2005a; Junge et al., 2001; Kalaba et al., 2016; Klinge et al., 1996; Ozog et al., 2014; Song et al., 2006; Williams et al., 1975). Therefore, mechanical requirements for surgical meshes are tough to settle and, to date, the parameters extracted from the mechanical characterization seem to have greater influence in device design and comparison than in *in-vivo* performance prediction. In addition, it should be noticed that recurrences and failures of hernia repairs are rarely caused by mesh rupture but usually result from mistakes during graft implantation or fixture (Cobb et al., 2005b). However, a crucial aspect of surgical meshes is the need to avoid alterations of the native tissue mobility after the implantation, and to promote the incorporation into native tissues. In this context, the stiffness and the anisotropy of the implant play a significant role in preventing hernia recurrence or patient discomfort (Kalaba et al., 2016; Konerding et al., 2011; Miao et al., 2015). The mesh stiffness and the dilatational strain evaluated in multiaxial test, such as ball burst test or biaxial test, are in our opinion the most suitable mechanical parameters for the evaluation of clinical outcomes, in terms of patient's comfort after implantation (Bilsel and Abci, 2012; Klosterhalfen et al., 2005; Mangera et al., 2012). The limits in the stiffness computed through uniaxial tensile test data are heightened by the reduced dimension specimens usually used in meshes uniaxial tensile test. However, the stiffness computed from uniaxial tensile test, even though not suitable as *in vivo* acceptability criterion, could be useful to assess the direction of graft implantation as well as anisotropy. On the contrary, thanks to its multiaxial pattern of solicitation, the membrane dilatational strain could be a stronger indicator of the mesh acceptability. Reference values can be found in literature where a range of elasticity between 11% and 32% is identified as physiologic for a tension of 16 N/cm and a value around 38% is determined for a tension of 32 N/cm (Bilsel and Abci, 2012; Junge et al., 2001).

5. Conclusions

To date, the lack of International Standards for surgical meshes testing leads to the use of dissimilar test protocols and to the extraction of not harmonized parameters in order to mechanically characterize these devices. Here, a test protocol composed of three quasi-static test methods is proposed with the aim of promoting its adoption in other laboratories. Accordingly, a meticulous description of set-ups, specifications and parameters computation is given, as well as drawings of the developed fixtures for a faithful reproduction. The test protocol, verified on 23 surgical meshes from different manufacturers, revealed easy to perform and highly replicable, with intra-subject variability characterized by coefficient of variations settled around 0.05. Its use within other laboratories could allow the determination of the inter-subject variability assessing its repeatability among users of alternative universal testing machines. Moreover, the collection of an extended set of data on surgical meshes evaluated with the same test protocol could lay the foundations for the definition of acceptability criteria and mechanical requirements for these implantable devices.

CRediT authorship contribution statement

Vittoria Civilini: Writing – original draft, Validation, Methodology, Formal analysis, Data curation. **Vincenzo Giacalone:** Writing – review & editing, Validation, Formal analysis. **Alberto L. Audenino:** Writing – review & editing, Methodology, Conceptualization. **Mara Terzini:** Writing – review & editing, Supervision, Methodology, Conceptualization.

Declaration of competing interest

The authors declare that they have no known competing financial interests or personal relationships that could have appeared to influence the work reported in this paper.

Data availability

Data will be made available on request.

Appendix A. Supplementary data

Supplementary data to this article can be found online at https://doi.org/10.1016/j.jmbbm.2023.105987.

References

Anurov, M.V., Titkova, S.M., Oettinger, A.P., 2012. Biomechanical compatibility of surgical mesh and fascia being reinforced: dependence of experimental hernia defect repair results on anisotropic surgical mesh positioning. Hernia 16, 199–210. https://doi.org/10.1007/s10029-011-0877-y.

Bilsel, Y., Abci, I., 2012. The search for ideal hernia repair; mesh materials and types. Int. J. Surg. 10, 317–321. https://doi.org/10.1016/j.ijsu.2012.05.002.

Cobb, W.S., Burns, J.M., Kercher, K.W., Matthews, B.D., James Norton, H., Todd Heniford, B., 2005a. Normal intraabdominal pressure in healthy adults. J. Surg. Res. 129, 231–235. https://doi.org/10.1016/j.jss.2005.06.015.

Cobb, W.S., Kercher, K.W., Heniford, B.T., 2005b. The argument for lightweight polypropylene mesh in hernia repair. Surg. Innovat. 12, 63–69. https://doi.org/10.1177/155335060501200109.

Coda, A., Lamberti, R., Martorana, S., 2012. Classification of prosthetics used in hernia repair based on weight and biomaterial. Hernia 16, 9–20. https://doi.org/10.1007/s10029-011-0868-z.

Cordero, A., Hernández-gascón, B., Pascual, G., Bellòn, J.M., Calvo, B., Peña, E., 2015. Biaxial Mechanical Evaluation of Absorbable and Nonabsorbable Synthetic Surgical Meshes Used for Hernia Repair : Physiological Loads Modify Anisotropy Response. https://doi.org/10.1007/s10439-015-1503-4.

De Maria, C., Santoro, V., Vozzi, G., 2016. Biomechanical, topological and chemical features that influence the implant success of an urogynecological mesh: a review. BioMed Res. Int. https://doi.org/10.1155/2016/1267521, 2016.

Deeken, C.R., Abdo, M.S., Frisella, M.M., Matthews, B.D., 2011a. Physicomechanical evaluation of absorbable and nonabsorbable barrier composite meshes for laparoscopic ventral hernia repair. Surg. Endosc. 25, 1541–1552. https://doi.org/10.1007/s00464-010-1432-0.

Deeken, C.R., Abdo, M.S., Frisella, M.M., Matthews, B.D., 2011b. Physicomechanical evaluation of polypropylene, polyester, and polytetrafluoroethylene meshes for inguinal hernia repair. J. Am. Coll. Surg. 212, 68–79. https://doi.org/10.1016/j.jamcollsurg.2010.09.012.

Deeken, C.R., Lake, S.P., 2017. Mechanical properties of the abdominal wall and biomaterials utilized for hernia repair. J. Mech. Behav. Biomed. Mater. 74, 411–427. https://doi.org/10.1016/j.jmbbm.2017.05.008.

Deeken, C.R., Thompson, D.M., Castile, R.M., Lake, S.P., 2014. Biaxial analysis of synthetic scaffolds for hernia repair demonstrates variability in mechanical anisotropy , non-linearity and hysteresis. J. Mech. Behav. Biomed. Mater. 38, 6–16. https://doi.org/10.1016/j.jmbbm.2014.06.001.

Dietz, H.P., Vancaillie, P., Svehla, M., Walsh, W., Steensma, A.B., Vancaillie, T.G., 2003. Mechanical properties of urogynecologic implant materials. Int. Urogynecol. J. 14, 239–243. https://doi.org/10.1007/s00192-003-1041-8.

Eliason, B.J., Frisella, M.M., Matthews, B.D., Deeken, C.R., 2011. Effect of repetitive loading on the mechanical properties of synthetic hernia repair materials. J. Am. Coll. Surg. 213, 430–435. https://doi.org/10.1016/j.jamcollsurg.2011.05.018.

Est, S., Roen, M., Chi, T., Simien, A., Castile, R.M., Thompson, D.M., Blatnik, J.A., Deeken, C.R., Lake, S.P., 2017. Multi-directional mechanical analysis of synthetic scaffolds for hernia repair. J. Mech. Behav. Biomed. Mater. 71, 43–53. https://doi.org/10.1016/j.jmbbm.2017.02.009.

Freytes, D.O., Rundell, A.E., Vande Geest, J., Vorp, D.A., Webster, T.J., Badylak, S.F., 2005. Analytically derived material properties of multilaminated extracellular matrix devices using the ball-burst test. Biomaterials 26, 5518–5531. https://doi.org/10.1016/j.biomaterials.2005.01.070.

Hernández-gascón, B., Peña, E., Melero, H., Pascual, G., Doblaré, M., Ginebra, M.P., 2011. Acta Biomaterialia Mechanical behaviour of synthetic surgical meshes. Finite element simulation of the herniated abdominal wall 7, 3905. https://doi.org/10.1016/j.actbio.2011.06.033. –3913.

Hollinsky, C., Sandberg, S., Koch, T., Seidler, S., 2008. Biomechanical properties of lightweight versus heavyweight meshes for laparoscopic inguinal hernia repair and their impact on recurrence rates. Surg. Endosc. Other Interv. Tech. 22, 2679–2685. https://doi.org/10.1007/s00464-008-9936-6.

Jones, K.A., Feola, A., Meyn, L., Abramowitch, S.D., Moalli, P.A., 2009. Tensile properties of commonly used prolapse meshes. Int. Urogynecol. J. 20, 847–853. https://doi.org/10.1007/s00192-008-0781-x.

Junge, K., Klinge, U., Prescher, A., Giboni, P., Niewiera, M., Schumpelick, V., 2001. Elasticity of the anterior abdominal wall and impact for reparation of incisional hernias using mesh implants. Hernia 5, 113–118. https://doi.org/10.1007/s100290100019.

Kalaba, S., Gerhard, E., Winder, J.S., Pauli, E.M., Haluck, R.S., Yang, J., 2016. Design strategies and applications of biomaterials and devices for Hernia repair. Bioact. Mater. 1, 2–17. https://doi.org/10.1016/j.bioactmat.2016.05.002.

Klinge, U., Conze, J., Limberg, W., Brücker, C., Ottinger, A.P., Schumpelick, V., 1996. [Pathophysiology of the abdominal wall]. Chirurg 67, 229–233.
Klinge, U., Klosterhalfen, B., 2012. Modified classiffication of surgical meshes for hernia repair based on the analyses of 1,000 explanted meshes. Hernia 16, 251–258. https://doi.org/10.1007/s10029-012-0913-6.
Klosterhalfen, B., Junge, K., Klinge, U., 2005. The lightweight and large porous mesh concept for hernia repair. Expet Rev. Med. Dev. 2, 103–117. https://doi.org/10.1586/17434440.2.1.103.
Klosterhalfen, B., Klinge, U., Schumpelick, V., Tietze, L., 2000. Polymers in hernia repair - common polyester vs. polypropylene surgical meshes. J. Mater. Sci. 35, 4769–4776. https://doi.org/10.1023/A:1004812410141.
Konerding, M.A., Bohn, M., Wolloscheck, T., Batke, B., Holste, J.L., Wohlert, S., Trzewik, J., Förstemann, T., Hartung, C., 2011. Maximum forces acting on the abdominal wall: experimental validation of a theoretical modeling in a human cadaver study. Med. Eng. Phys. 33, 789–792. https://doi.org/10.1016/j.medengphy.2011.01.010.
Lerdsirisopon, S., Frisella, M.M., Matthews, B.D., Deeken, C.R., 2011. Biomechanical evaluation of potential damage to hernia repair materials due to fixation with helical titanium tacks. Surg. Endosc. 25, 3890–3897. https://doi.org/10.1007/s00464-011-1816-9.
Li, X., Kruger, J., Jor, J., Nielsen, P., Nash, M., Wong, V., Dietz, H.P., 2014. Characterizing the ex vivo mechanical properties of synthetic polypropylene surgical mesh. J. Mech. Behav. Biomed. Mater. 37, 48–55. https://doi.org/10.1016/j.jmbbm.2014.05.005.
Mangera, A., Bullock, A.J., Chapple, C.R., MacNeil, S., 2012. Are biomechanical properties predictive of the success of prostheses used in stress urinary incontinence and pelvic organ prolapse? A systematic review. Neurourol. Urodyn. 31, 13–21. https://doi.org/10.1002/nau.21156.
Martin, D.P., Badhwar, A., Shah, D.V., Rizk, S., Eldridge, S.N., Gagne, D.H., Ganatra, A., Darois, R.E., Williams, S.F., Tai, H.C., Scott, J.R., 2013. Characterization of poly-4-hydroxybutyrate mesh for hernia repair applications. J. Surg. Res. 184, 766–773. https://doi.org/10.1016/j.jss.2013.03.044.
Maurer, M.M., Röhrnbauer, B., Feola, A., Deprest, J., Mazza, E., 2015. Prosthetic meshes for repair of hernia and pelvic organ prolapse: comparison of biomechanical properties. Materials (Basel) 8, 2794–2808. https://doi.org/10.3390/ma8052794.
Maurer, M.M., Röhrnbauer, B., Feola, A., Deprest, J., Mazza, E., 2014. Mechanical biocompatibility of prosthetic meshes: a comprehensive protocol for mechanical characterization. J. Mech. Behav. Biomed. Mater. 40, 42–58. https://doi.org/10.1016/j.jmbbm.2014.08.005.
Miao, L., Wang, F., Wang, L., Zou, T., Brochu, G., Guidoin, R., 2015. Physical characteristics of medical textile prostheses designed for hernia repair: a comprehensive analysis of select commercial devices. Materials (Basel) 8, 8148–8168. https://doi.org/10.3390/ma8125453.
Moalli, P.A., Papas, N., Menefee, S., Albo, M., Meyn, L., Abramowitch, S.D., 2008. Tensile properties of five commonly used mid-urethral slings relative to the TVT™. Int. Urogynecol. J. 19, 655–663. https://doi.org/10.1007/s00192-007-0499-1.
Ozog, Y., Deprest, J., Haest, K., Claus, F., De Ridder, D., Mazza, E., 2014. Calculation of membrane tension in selected sections of the pelvic floor. Int. Urogynecol. J. 25, 499–506. https://doi.org/10.1007/s00192-013-2253-1.
Pott, P.P., Schwarz, M.L.R., Gundling, R., Nowak, K., Hohenberger, P., Roessner, E.D., 2012. Mechanical properties of mesh materials used for hernia repair and soft tissue augmentation. PLoS One 7, 1–10. https://doi.org/10.1371/journal.pone.0046978.
Rastegarpour, A., Cheung, M., Vardhan, M., Ibrahim, M.M., Butler, C.E., Levinson, H., 2016. Surgical mesh for ventral incisional hernia repairs: understanding mesh design. Can. J. Plast. Surg. 24, 41–50. https://doi.org/10.1177/229255031602400110.
Ruiz-zapata, A.M., Feola, A.J., Heesakkers, J., Graaf, P. De, 2018. Biomechanical properties of the pelvic Floor and its relation to pelvic Floor disorders. Eur. Urol. Suppl. 17, 80–90. https://doi.org/10.1016/j.eursup.2017.12.002.
Saberski, E.R., Orenstein, S.B., Novitsky, Y.W., 2011. Anisotropic evaluation of synthetic surgical meshes. Hernia 15, 47–52. https://doi.org/10.1007/s10029-010-0731-7.
Sahoo, S., Delozier, K.R., Erdemir, A., Derwin, K.A., 2015. Clinically relevant mechanical testing of hernia graft constructs. J. Mech. Behav. Biomed. Mater. 41, 177–188. https://doi.org/10.1016/j.jmbbm.2014.10.011.
Shepherd, J.P., Feola, A.J., Abramowitch, S.D., Moalli, P.A., 2012. Uniaxial biomechanical properties of seven different vaginally implanted meshes for pelvic organ prolapse. Int. Urogynecol. J. 23, 613–620. https://doi.org/10.1007/s00192-011-1616-8.
Soares, B.M., Guidoin, R.G., Marois, Y., Martin, L., King, M.W., Laroche, G., Zhang, Z., Charara, J., Girard, J.F., 1996. In vivo characterization of a fluoropassivated gelatin-impregnated polyester mesh for hernia repair. J. Biomed. Mater. Res. 32, 293–305. https://doi.org/10.1002/(SICI)1097-4636(199611)32:3<293::AID-JBM2>3.0.CO;2-N.
Song, C., Alijani, A., Frank, T., Hanna, G.B., Cuschieri, A., 2006. Mechanical properties of the human abdominal wall measured in vivo during insufflation for laparoscopic surgery. Surg. Endosc. Other Interv. Tech. 20, 987–990. https://doi.org/10.1007/s00464-005-0676-6.
Todros, S., Pachera, P., Pavan, P.G., Natali, A.N., 2018. Investigation of the mechanical behavior of polyester meshes for abdominal surgery: a preliminary study. J. Med. Biol. Eng. 38, 654–665. https://doi.org/10.1007/s40846-017-0337-y.
Todros, S., Pavan, P.G., Pachera, P., Natali, A.N., 2017. Synthetic surgical meshes used in abdominal wall surgery: Part II—biomechanical aspects. J. Biomed. Mater. Res. - Part B Appl. Biomater. 105, 892–903. https://doi.org/10.1002/jbm.b.33584.
Velayudhan, S., Martin, D., Cooper-White, J., 2009. Evaluation of dynamic creep properties of surgical mesh prostheses - uniaxial fatigue. J. Biomed. Mater. Res. - Part B Appl. Biomater. 91, 287–296. https://doi.org/10.1002/jbm.b.31401.
Williams, J.F., Kirkpatrick, J., Syme, G.A., 1975. Force measurement in the abdominal wall. Biomed. Eng. 10, 181–183.
Wolf, M.T., Carruthers, C.A., Dearth, C.L., Crapo, P.M., Huber, A., Burnsed, O.A., Londono, R., Johnson, S.A., Daly, K.A., Stahl, E.C., Freund, J.M., Medberry, C.J., Carey, L.E., Nieponice, A., Amoroso, N.J., Badylak, S.F., 2013. Polypropylene surgical mesh coated with extracellular matrix mitigates the host foreign body response 001026, 234–246. https://doi.org/10.1002/jbm.a.34671.
Wolloscheck, T., Gaumann, A., Terzic, A., Heintz, A., Junginger, T., Konerding, M.A., 2004. Inguinal hernia: measurement of the biomechanics of the lower abdominal wall and the inguinal canal. Hernia 8, 233–241. https://doi.org/10.1007/s10029-004-0224-7.
Zhu, L.-M., 2015. Mesh implants: an overview of crucial mesh parameters. World J. Gastrointest. Surg. 7, 226. https://doi.org/10.4240/wjgs.v7.i10.226.